Report

Cell Reports

Molecular Mechanism for Ligand Recognition and Subtype Selectivity of α_{2C} Adrenergic Receptor

Graphical Abstract

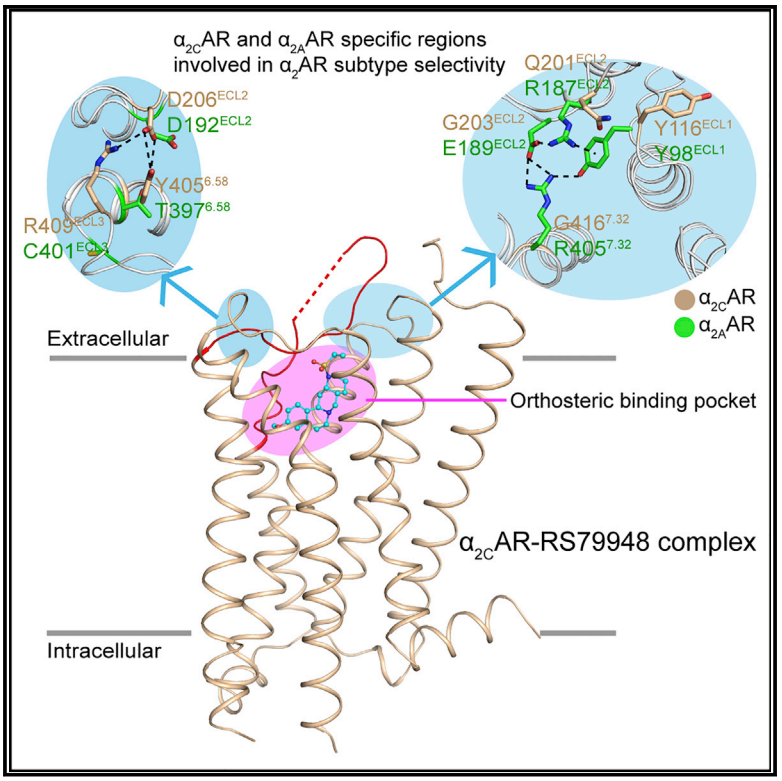

Highlights

- Crystal structure of human α_{2C}AR in complex with RS79948 is solved
- A specific loosened helix at the top of TM4 in α_{2C}AR is involved in receptor activation
- Extracellular regions play a role in determining α_2 adrenergic subtype selectivity

Authors

Xiaoyu Chen, Yueming Xu, Lu Qu, ..., Suwen Zhao, Dong Wu, Guisheng Zhong

Correspondence

zhaosw@shanghaitech.edu.cn (S.Z.), wudong@shanghaitech.edu.cn (D.W.), zhongsh@shanghaitech.edu.cn (G.Z.)

In Brief

Chen et al. report the crystal structure of human α_{2C}AR and the functional experimental results, which indicate that extracellular regions determine α_2 adrenergic subtype selectivity. The structural and functional results provide the molecular explanation for α_{2C}AR selective ligands and insights to understand GPCR subtype selectivity.

Chen et al., 2019, Cell Reports *29*, 2936–2943
December 3, 2019
https://doi.org/10.1016/j.celrep.2019.10.112

CellPress

OPEN ACCESS
CellPress

Cell Reports
Report

Molecular Mechanism for Ligand Recognition and Subtype Selectivity of α_{2C} Adrenergic Receptor

Xiaoyu Chen,[1,2,3,4,10] Yueming Xu,[1,10] Lu Qu,[1,4,5] Lijie Wu,[1] Gye Won Han,[6] Yu Guo,[1,2,4] Yiran Wu,[1] Qingtong Zhou,[1] Qianqian Sun,[1] Cenfeng Chu,[1,2,4] Jie Yang,[1,2,4] Liu Yang,[1,2,4] Quan Wang,[1,2,4] Shuguang Yuan,[7,8] Ling Wang,[1] Tao Hu,[1,2,3,4] Houchao Tao,[1] Yaping Sun,[9] Yunpeng Song,[9] Liaoyuan Hu,[9] Zhi-Jie Liu,[1,2] Raymond C. Stevens,[1,2] Suwen Zhao,[1,2,*] Dong Wu,[1,*] and Guisheng Zhong[1,2,11,*]

[1]iHuman Institute, ShanghaiTech University, Shanghai 201210, China
[2]School of Life Science and Technology, ShanghaiTech University, Shanghai 201210, China
[3]CAS Center for Excellence in Molecular Cell Science, Shanghai Institute of Biochemistry and Cell Biology, Chinese Academy of Sciences, Shanghai, China
[4]University of Chinese Academy of Sciences, Beijing 100049, China
[5]National Laboratory of Biomacromolecules, Institute of Biophysics, Chinese Academy of Sciences, Beijing 100101, China
[6]Departments of Biological Sciences and Chemistry, Bridge Institute, University of Southern California, Los Angeles, CA 90089, USA
[7]Shenzhen Institutes of Advanced Technology, Chinese Academy of Sciences, Shenzhen 518055, China
[8]Laboratory of Biomodelling, Faculty of Chemistry & Biological and Chemical Research Centre, University of Warsaw, 02-093 Warsaw, Poland
[9]Amgen Asia R&D Center, Amgen Biopharmaceutical R&D (Shanghai), Shanghai 201210, China
[10]These authors contributed equally
[11]Lead Contact
*Correspondence: zhaosw@shanghaitech.edu.cn (S.Z.), wudong@shanghaitech.edu.cn (D.W.), zhongsh@shanghaitech.edu.cn (G.Z.)
https://doi.org/10.1016/j.celrep.2019.10.112

SUMMARY

Adrenergic G-protein-coupled receptors (GPCRs) mediate different cellular signaling pathways in the presence of endogenous catecholamines and play important roles in both physiological and pathological conditions. Extensive studies have been carried out to investigate the structure and function of β adrenergic receptors (βARs). However, the structure of α adrenergic receptors (αARs) remains to be determined. Here, we report the structure of the human α_{2C} adrenergic receptor (α_{2C}AR) with the non-selective antagonist, RS79948, at 2.8 Å. Our structure, mutations, modeling, and functional experiments indicate that a α_{2C}AR-specific $D206^{ECL2}$-$R409^{ECL3}$-$Y405^{6.58}$ network plays a role in determining α_2 adrenergic subtype selectivity. Furthermore, our results show that a specific loosened helix at the top of TM4 in α_{2C}AR is involved in receptor activation. Together, our structure of human α_{2C}AR-RS79948 provides key insight into the mechanism underlying the α_2 adrenergic receptor activation and subtype selectivity.

INTRODUCTION

Adrenergic receptors can be classified into two subgroups: αARs and βARs (Ahlquist, 1948, 1962, 1967), with the former further divided into α_1ARs and α_2ARs. α_1ARs, α_2ARs, and βARs trigger G_q, G_i, and G_s proteins, respectively, when activated by two main endogenous ligands, epinephrine and norepinephrine. Activation of βARs results in the increase of heart rate, contractile force, and the relaxation of smooth muscle, while activation of α_1ARs leads to vasoconstriction of vascular smooth muscle. α_2ARs, as presynaptic inhibitory receptors, are important for regulating catecholamine signaling (Bücheler et al., 2002; MacDonald et al., 1997). In humans, α_2ARs are divided further into three subtypes: α_{2A}AR, α_{2B}AR, and α_{2C}AR. α_{2A}AR and α_{2C}AR both regulate the release of norepinephrine but at high and low stimulation frequencies, respectively (Hein et al., 1999). α_{2C}AR possesses some unique properties. It displays dominant intracellular distribution in fibroblasts and vascular smooth muscle cells, compared with strong plasma membrane localization in neuronal or endocrine cells (Angelotti et al., 2010; Daunt et al., 1997; Filipeanu et al., 2011; Hurt et al., 2000). Interestingly, α_{2C}AR is sensitive to decreased environmental temperature and it is transported to the cell surface during exposure to temperatures down to 28–30°C (Chotani and Flavahan, 2011; Chotani et al., 1999; Filipeanu et al., 2011, 2015; Honda et al., 2007; Jeyaraj et al., 2001). This sensitivity explains α_{2C}AR's role in Raynaud's syndrome, a disease associated with cold exposure (Chotani et al., 2000; Filipeanu, 2015).

Although the three α_2AR subtypes differ considerably in their tissue distribution and physiological roles, they are highly homologous in the trans-membrane region and thus share most agonists and antagonists, limiting receptor-specific research to genetic modification in animals (Brede et al., 2002, 2003; Hein et al., 1999; Kable et al., 2000; Moura et al., 2006) and *in vitro* investigations in cell lines. Clearly, the ability to selectively target the α_2AR subtypes would have important benefits on further *in vivo* study for α_2ARs. Unfortunately, the source of this subtype selectivity is not well understood. To this end, we solved the crystal structure of human α_{2C}AR in complex with RS79948, a non-selective antagonist of α_2ARs. Based on the solved structure, two selective antagonists, JP1302 and OPC-28326, were docked into α_{2C}AR, and, supported by mutagenesis, modeling,

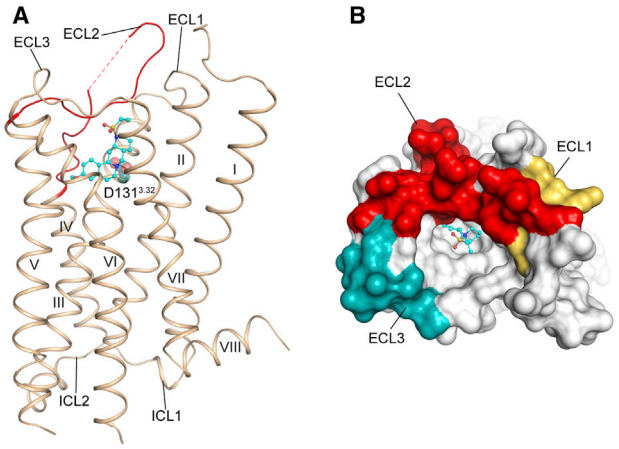

Figure 1. Overall Structure of the α_{2C}AR-RS79948 Complex

(A) Side view of α_{2C}AR-RS79948 complex. α_{2C}AR is shown in wheat cartoon representation; RS79948 is shown as cyan balls and sticks; ECL2 is shown in red; and D131$^{3.32}$ is shown as spheres with carbons in green.

(B) Top view of α_{2C}AR-RS79948 complex with receptor shown in surface representation. ECL1, ECL2, and ECL3 are shown as yellow, red, and blue, respectively. See Figures S1 and S2.

functional assays, and comparison with other aminergic receptors, we are able to provide key insight into the subtype selectivity of α_2ARs.

RESULTS

α_{2C}AR Displays a Prototypical Class-A G-Protein-Coupled Receptor Atomic Structure

We carried out structural studies using an engineered human α_{2C}AR construct with modifications as detailed in Figure S1. Proteins were purified and crystallized in complex with RS79948. The binding affinity of RS79948 with this engineered α_{2C}AR protein was comparable to that with the wild-type receptor (Figures S1E and S1F). The crystal structure of the α_{2C}AR-RS79948 complex, which was determined at 2.8-Å resolution (Table S1), was found to exhibit a canonical class A G-protein-coupled receptor (GPCR) architecture, including a seven-transmembrane helical bundle (TM I–VII) linked by three extracellular (ECL1–3) and three intracellular (ICL1–3) loops, and a four-residue truncated helix VIII (Figure 1). The α_{2C}AR-RS79948 complex displayed the typical inactive state structure of class A GPCRs, i.e., the intracellular helical arrangements and microswitches were consistent with the β_2AR structure in an inactive-like state (PDB: 2RH1, 3SN6) (Cherezov et al., 2007; Rasmussen et al., 2011) (Figure S2).

α_{2C}AR Shows a Highly Hydrophobic Pocket

RS79948 is a non-selective high-affinity α_2AR antagonist belonging to non-imidazoline class and forms a conserved salt bridge with the carboxylate group of D131$^{3.32}$ in pocket (Figure 2A). Electron density of RS79948 and surrounding residues at this area are included (Figure S3). Besides the polar binding with D131$^{3.32}$, RS79948 is surrounded by seven aromatic residues on TM6 and TM7, and L204$^{45.52}$ at the center of the pocket forming the hydrophobic environment of the pocket (Figure 2A). RS79948 forms cation-π and π-π interactions with F398$^{6.51}$ and another cation-π with F423$^{7.39}$ (Figure 2B). α_{2C}AR L204$^{45.52}$I has no effect on UK14,304 but decreases the potency of RS79948, suggesting L204$^{45.52}$ plays a role in determining subtype selectivity (Figure 2B). Furthermore, L128$^{3.29}$, as part of the hydrophobic barrier, is a selective ligand binding site since L128$^{3.29}$A or L128$^{3.29}$W significantly attenuates the antagonism of RS79948, while it has no effect on UK14,304 (Figures 2B and 2C).

Structure Comparison between α_{2C}AR and Other Aminergic Receptors

Next, we compared the pocket shapes of our solved structure, the ligand positions, and the features of the extracellular parts to other aminergic receptors (Cherezov et al., 2007; Chien et al., 2010; Haga et al., 2012; Ishchenko et al., 2017; Kruse et al., 2012; Peng et al., 2018; Shimamura et al., 2011; Thal et al., 2016; Wang et al., 2017, 2018; Warne et al., 2012; Yin et al., 2018) (Figure 3). RS79948 in α_{2C}AR occupied a relatively shallow position (Figure S4), suggesting that α_{2C}AR antagonists may be more impacted by extracellular parts than most of the other aminergic receptors. Likewise, pocket shapes differed especially between subfamilies, while their volumes were comparable, likely due to the conservation of aminergic GPCRs (Figure S4). ECLs play an important role during receptor-ligand association and ligand binding and possess much more diversity than transmembrane regions among solved aminergic receptors (Figure 3). In our α_{2C}AR structure, two disulfide bonds exist in the extracellular region of α_{2C}AR: C124$^{3.25}$–C202$^{45.50}$ and C408$^{6.61}$–C412^{ECL3}. The former, constraining ECL2 to TM3, is conserved in most GPCRs and disruption of this disulfide bond often impairs agonist binding affinity. Moreover, the C$^{3.25}$–C$^{45.50}$ separates ECL2 into two segments. The segment between C$^{45.50}$ and TM5 is directly involved in ligand binding, like L204$^{45.52}$ in α_{2C}AR (Figure 2). Another segment between TM4 and C$^{45.50}$ is more diverse and flexible. Notably, even a small change in its length and flexibility can impact the activation of α_{2C}AR.

A difference at the top of TM4 in α_{2C}AR, compared to other aminergic receptors, is the loosened helix. This is likely caused by the existence of two prolines PP (185$^{4.59}$, 186$^{4.60}$). The P185L mutation on α_{2C}AR was predicted to regain the helical structure at the top of TM4 considering the similar sequence and typical helix structure in β_2AR-TM4 (Figures S5A and S5B), which may shorten ECL2 and decrease its flexibility. The P185L mutation attenuated the potency of the two endogenous agonists, norepinephrine and epinephrine (Figure S5C), suggesting that appropriate flexibility of ECL2 may be necessary for GPCR activation. However, the P185L mutation seemed to have much less effect on α_2-agonists, such as clonidine and dexmedetomidine (Figure S5), which had no hydroxyl group on the benzene ring and thus had less interactions with TM5 linked with ECL2. This indicated that the loosened helix on TM4 may be specifically involved in the receptor activation triggered by norepinephrine and epinephrine.

Despite the low sequence identity among αARs and βARs, they all target endogenous ligands epinephrine and norepinephrine. When comparing α_{2C}AR with other solved aminergic receptors, we found three reasonable similar structures: α_{2A}AR

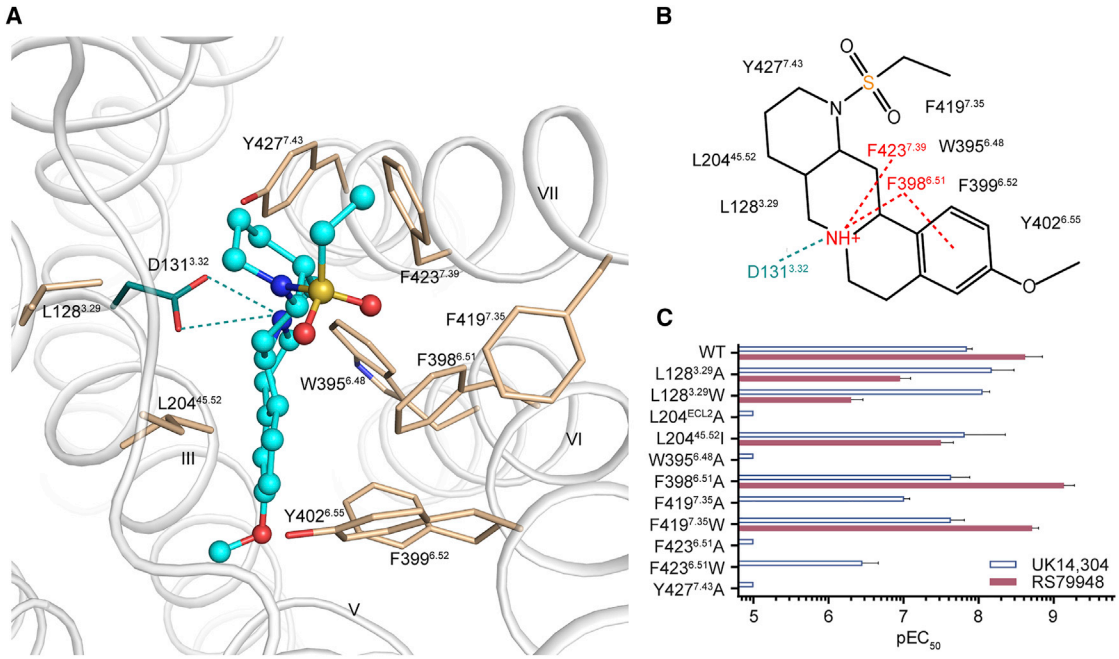

Figure 2. Analysis of the RS79948 Binding Pocket of α_{2C}AR

(A) Key residues (green and wheat sticks) involved in RS79948 (cyan spheres and sticks) binding. See Figure S3 and Table S1.

(B) Schematic representation of the interactions between α_{2C}AR and RS79948. The salt bridge is shown as green dashed line, and π-π interaction and cation-π interaction are shown as red dashed lines.

(C) Mutation analysis of binding pocket key residues by cAMP assay. The potency of UK14,304 and RS79948 as determined by comparison of the negative logarithm of the EC_{50} (pEC_{50}) values (data are mean ± SEM; $n \geq 3$). Statistical analyses of RS79948 were not performed on L204A, W395A, F419A, F423A, F423W, and Y427A as they show inconsistent response to UK14,304 compared to wild-type (WT) α_{2C}AR.

See Table S2.

(root-mean-square deviation [RMSD]: 0.971), β_1AR (PDB: 5A8E; Sato et al., 2015; RMSD: 1.389), and β_2AR (PDB: 2RH1; RMSD: 1.343). Among the 12 defined aminergic orthosteric binding sites (OBSs) (3.32, 3.33, 3.36, 45.52, 5.42, 5.46, 6.48, 6.51, 6.52, 6.55, 7.39, and 7.43) (Michino et al., 2015), 8 sites are conserved in adrenergic receptors (Figure S6A). D3.32, S5.42, S5.46, Y7.43, forming H-bonds with epinephrine (in β_2AR-epinephrine structure; PDB: 4LDO) (Ring et al., 2013), are identical in the nine adrenergic receptors, despite specific residues at 6.55 and 7.39 forming additional H-bonds in βARs (Figure S6B). In the α_{2C}AR-epinephrine docking model, Y6.55 forms H-bond with epinephrine, similar to N6.55 in β_2AR (4LDO).

Subtype Adrenergic Selectivity Can Be Achieved by Targeting Extracellular Loops

When we further compared the structure of α_{2C}AR-RS79948 and α_{2A}AR-RS79948 (PDB: 6KUX) (L Qu, Q.Z., Y.X., Y.G., X.C., G.W.H., Z.J.L., R.C.S., G.Z., D.W., and S.Z., unpublished data), we found that RS79948 interacts with almost the same binding sites, except for the residue at 45.52 which is L in α_{2C}AR and I in α_{2A}AR (Figure S7A). Also, OPC-28326, an α_{2C}AR selective antagonist with about 40-fold lower affinity on α_{2A}AR, docked into both α_{2C}AR and α_{2A}AR bound to similar orthosteric pocket sites, ignoring some unshown extracellular residues (Figure S7B). This finding supports the conclusion that subtype selectivity does not come from the orthosteric pockets. The ECL3 region ^{408}CREAC^{412} in α_{2C}AR was found differing from that in α_{2A}AR, creating a kink in the loop that orients R409 ^{ECL3} to interact with D206^{ECL2} and another unique residue that we discuss below.

To reveal the molecular basis in the orthosteric pocket for which JP1302 selectively binds α_{2C}AR rather than α_{2A}AR, we performed molecular-docking-guided mutagenesis study. JP1302 competitively binds the orthosteric pocket of α_{2C}AR (Figures S8A and S8B). There are two positively charged amine groups on JP1302 that may interact with D131$^{3.32}$. To verify which nitrogen atom was involved in this interaction, a new molecule named TC1515 was synthesized with the 1-methylpiperazine group of JP1302 changed to morpholine and TC1515 did not exhibit the antagonism on α_{2C}AR (Figures S8C and S8D). This result is consistent with one of the molecule docking pose of JP1302 (Figures S8E and S8F). This model explains why L128$^{3.29}$A attenuated the potency of RS79948 but does not affect JP1302, while another mutation L128$^{3.29}$W with larger side chain slightly increases the potency of JP1302 (Figure S8E; Table S2). Notably, F419$^{7.35}$W enhances the binding by, perhaps, stronger T-shape π-π interaction. More importantly, the positively charged amine group in the 2,3-benzoquinoline of JP1302 displays a salt bridge with D206^{ECL2} and cation-π interaction with Y405$^{6.58}$, a unique residue among aminergic receptors.

Given the unique configuration of the extracellular domains of α_{2C}AR, we hypothesized that ligand subtype selectivity may be due to these differences. α_{2C}AR has a specialized interaction

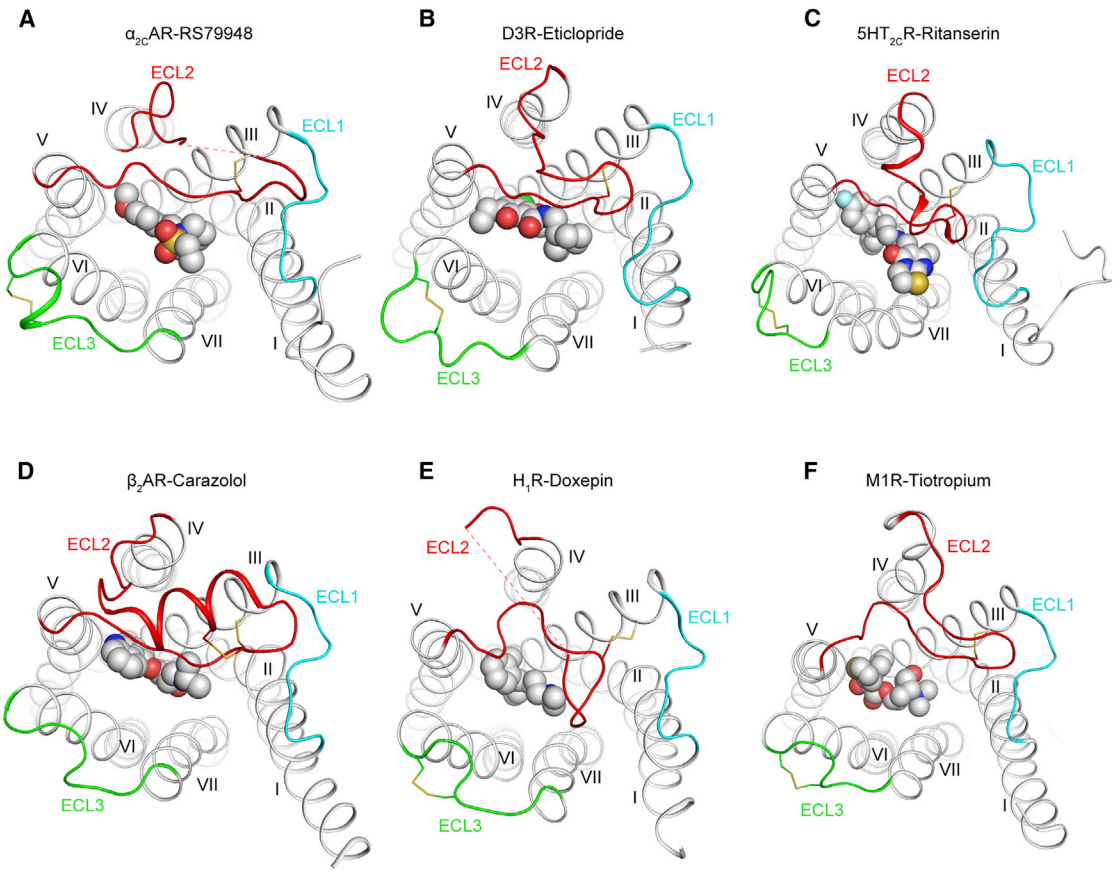

Figure 3. Extracellular Loops in the Structures of Aminergic Receptors in Extracellular View

(A–F) Receptors are shown as gray cartoons. α_{2C}AR (A), β_2AR (2RH1) (B), D3R (3PBL) (C), H_1R (3RZE) (D), M1R (5CXV) (E), and $5HT_{2C}$R (6BQH) (F). The extracellular loops, ECL1, ECL2, and ECL3, in each structure are colored cyan, red, and green, respectively. The ligands are shown as gray spheres.
See Figures S4–S6.

network formed by $D206^{ECL2}$, $R409^{ECL3}$, and $Y405^{6.58}$ that does not exist in α_{2A}AR (Figure 4A). Each of the three mutations and the triple mutation had no effect on RS79948 (Figure 4B). Although among the three point mutations, only Y405T slightly reduced the potency of JP1302, the triple mutation abolished JP1302's and OPC-28326's effect, implying that these sites and their network may be critical to the ligands specific to this subtype. In addition, the α_{2A}AR structure-based model with the complementary side chains of $Y98^{ECL1}$, $E189^{ECL2}$, and $R405^{7.32}$ showed that there may be a different interaction network in α_{2A}AR formed by $Y98^{ECL1}$, $R187^{ECL2}$, $E189^{ECL2}$, and $R405^{7.32}$ acting as a lid that covers the entrance of the ligand binding pocket (Figure 4C). This may block out big molecules like JP1302 and OPC-28326 that conversely will settle into the α_{2C}AR pocket through an unimpeded entrance. Thus, we were able to design and build an engineered α_{2A}AR to restore JP1302/OPC-28326 antagonism on it.

We hypothesized that a α_{2A}AR chimera, with the α_{2A}AR "lid" disabled ($R405^{7.32}$G) and the α_{2C}AR unique network added (the ECL3 nearby part of α_{2A}AR, $T397^{6.58}$-$P404^{ECL3}$, replaced with the corresponding part of α_{2C}AR, $Y405^{6.58}$-$P415^{7.31}$), may allow JP1302 and OPC-28326 to settle in the α_{2A}AR chimera pocket (Figure 4D). The additional mutation, K144A, was introduced in to remove interference of high-concentration-agonist-induced G_s signaling, which was demonstrated in α_{2A}AR (L Qu, Q.Z., Y.X., Y.G., X.C., G.W.H., Z.J.L., R.C.S., G.Z., D.W., and S.Z., unpublished data). The functional assay showed that JP1302 and OPC-28326 displayed good antagonism effects on the α_{2A}AR-chimera. Moreover, α_{2A}AR-R405G and chimera-G408R (both with K144A) had partial rescue compared with α_{2A}AR-chimera. This experiment supports our hypothesis that the "lid" in the α_{2A}AR pocket entrance shut out JP1302 and OPC-28326 and that the network at the α_{2C}AR pocket edge interacted with the two selective antagonists (Figures 4E and 4F).

DISCUSSION

In this study, we solved the crystal structure of human α_{2C}AR-RS79948, which provides some insight for understanding receptor-ligand interaction and subtype selectivity. The differences between α and β adrenergic receptors were identified by distinct potency of agonists (Ahlquist, 1948). Based on α_{2C}AR-RS79948 atomic structure, we docked a native ligand epinephrine into the pocket and investigated the similarity between αARs and βARs

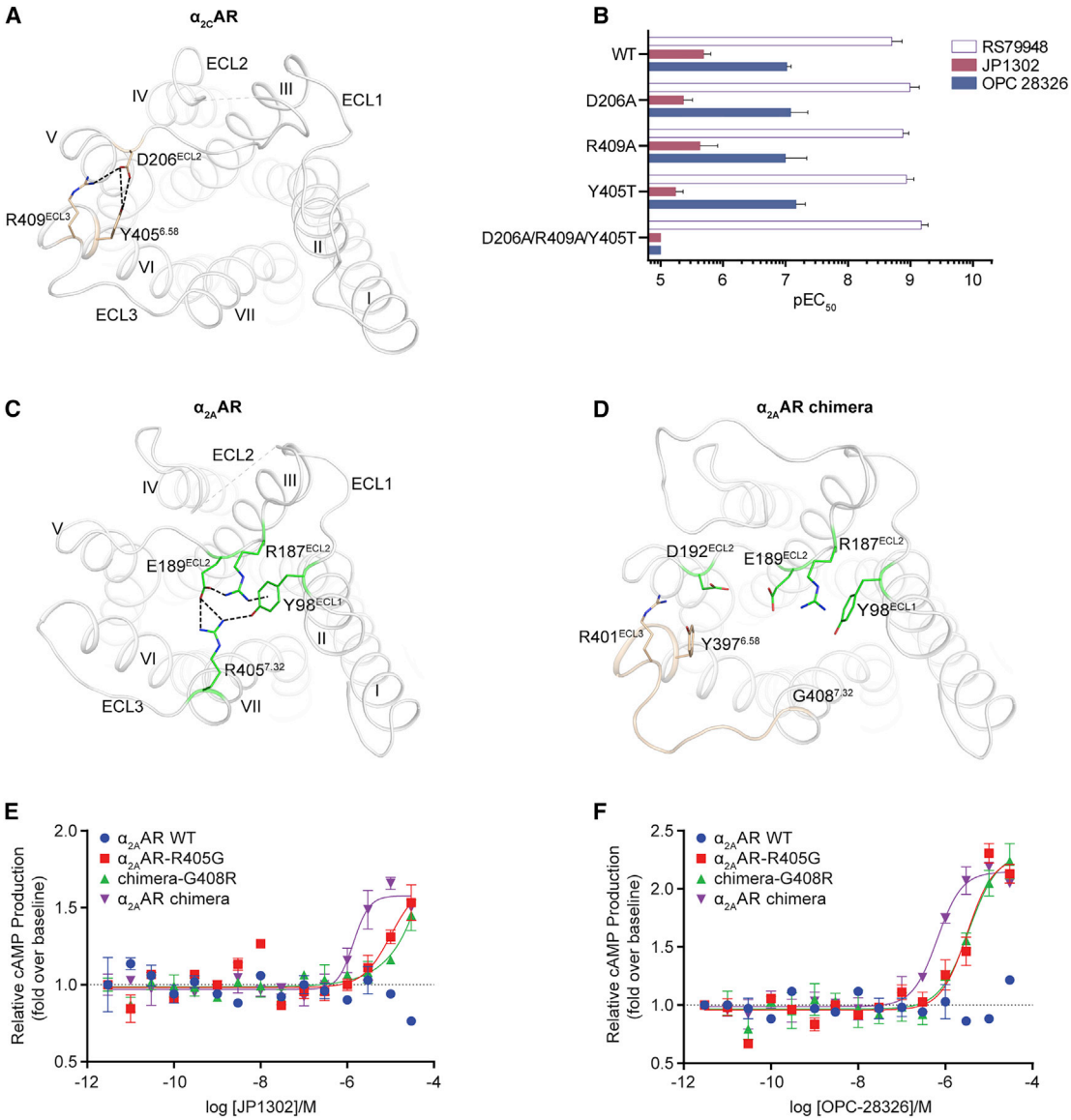

Figure 4. Subtype Selectivity Studies on α_{2C}AR through JP1302 and OPC-28326

See Figures S7 and S8.

(A) The unique interaction network formed by D206^{ECL2}, R409^{ECL3}, and Y405$^{6.58}$ in α_{2C}AR is displayed as a black dashed line.

(B) The potency comparison of RS79948, JP1302, and OPC-28326 on α_{2C}AR WT and mutations. The results of cAMP assay are shown as pEC_{50} values (data are mean ± SEM; n ≥ 3). The pEC_{50} values of JP1302 and OPC-28326 on D206A/R409A/Y405T were estimated at >5 μM due to a lack of response and non-convergence of the data to nonlinear regression analysis.

(C) Interaction network formed by Y98^{ECL1}, R187^{ECL2}, E189^{ECL2}, and R405$^{7.32}$ in the α_{2A}AR model with side chains of Y98^{ECL1}, E189^{ECL2}, and R405$^{7.32}$ computed based on α_{2A}AR structure.

(D) Predicted structure of α_{2A}AR chimera with T397-R405 replaced by α_{2C}AR Y405-G416, which were renumbered as Y397-G408 and are shown in wheat.

(E and F) α_{2A}AR R405G, α_{2A}AR chimera, and chimera G408R (all with additional K144A) allowed JP1302 (E) and OPC-28326 (F) to display antagonism on clonidine (10 μM)-induced cAMP inhibition compared to α_{2A}AR WT. Data are shown as mean ± SEM with three independent experiments performed in triplicate.

for their recognition to the same endogenous ligands. Besides, earlier functional studies showed that the position 7.39, which is F in αARs and N in βARs, may play a critical role in determining the selectivity between α and β adrenergic receptors. N312$^{7.39}$Q and N312$^{7.39}$T mutants in β_2AR increased the binding affinity of α_2-antagonists yohimbine and *para*-aminoclodine (Suryanarayana and Kobilka, 1993), while F412$^{7.39}$N in α_{2A}AR significantly increased the affinity of dihydroalprenolol, a β_2-antagonist (Suryanarayana et al., 1991). The property and proper size of N7.39 is important for β-selective ligands with ethanolamine backbones and bigger substitutions on the amine, from isopropyl (isoprenaline, alprenolol) to aromatic rings (salmeterol, carvedilol).

In βARs, H-bonds were formed between the residues S5.42, S5.46, and the *meta* hydroxyl, *para* hydroxyl on the benzene ring of most agonists. These bindings were found to be necessary for the receptor activation (Sato et al., 1999). Typical α_1-agonists such as phenylephrine, xymetazoline, and A61603, only contained a *meta* hydroxyl on the benzene ring, which was supposed to interact with S5.42 (Hwa and Perez, 1996). It was suggested that the polar interaction between agonists and TM5 was important for activation of adrenergic receptors. Notably, α_2 agonists did possess the hydroxyl groups on the benzene ring, but the α_2 receptor activation was not affected, suggesting that additional mechanism may underlie its activation.

Interestingly, our structure of human α_{2C}AR-RS79948 indicated that a loosened helix at the top of TM4 specifically existed in α_2ARs, which was involved in regulating the ligand binding and receptor activation. The helix structure was hypothesized to be regained by P185L of α_{2C}AR. Our functional results showed that the potency of epinephrine and norepinephrine was significantly reduced, while α_2-agonists clonidine and dexmedetomidine, without the hydroxyl group, showed no or slight potency reduction on α_{2C}AR-P185L. We reasoned that hydroxyl groups of epinephrine and norepinephrine formed H-bond with TM5, and the change of loosened helix of TM4 induced a change of ECL2, which was directly involved in ligand binding. The loosened helix at TM4 of α_2ARs is an elaborate change in evolution of GPCR and plays a specific role in the receptor activation of α_2ARs.

Moreover, despite the highly conserved pocket, the molecular basis of selectivity between α_{2C}AR and α_{2A}AR was revealed by docking model, mutations, and the α_{2A}AR-chimera. The triple mutation D206A/R409A/Y405T abolished the function of JP1302 and OPC-28326 while it had no effect on nonselective UK14,304 and RS79948, suggesting that the network found in the structure was crucial for α_{2C}AR selectivity. In the α_{2A}AR-chimera protein, we reliably reproduced the antagonism of α_{2C}AR selective antagonists on α_{2A}AR by removing the α_{2A}AR-specific "lid" and adding α_{2C}AR-specific $D206^{ECL2}$-$R409^{ECL3}$-$Y405^{6.58}$ network. Our structural and functional results provided molecular foundation for α_{2C}AR selective ligands beneficial to *in vivo* subtype functional study and new insights to understanding GPCR subtype selectivity.

STAR★METHODS

Detailed methods are provided in the online version of this paper and include the following:

- KEY RESOURCES TABLE
- LEAD CONTACT AND MATERIALS AVAILABILITY
- EXPERIMENTAL MODEL AND SUBJECT DETAILS
  - Cell Lines
  - Method Details
  - Engineering of Human ADRA2C for Structure Determination
  - Protein Expression in sf9 Insect Cell Line
  - Protein Purification
  - Lipidic Cubic Phase Crystallization
  - Data Collection and Structure Determination
  - Radioligand Binding Assay
  - Cell Culture and Transfection
  - Split Luciferase Biosensor cAMP Assay
  - Epinephrine, JP1302, and OPC-28326 Docking to α_{2A}AR and α_{2C}AR
  - Calculation of Binding Pocket's Volume
  - Calculation of RMSD
- QUANTIFICATION AND STATISTICAL ANALYSIS
- DATA AND CODE AVAILABILITY

SUPPLEMENTAL INFORMATION

Supplemental Information can be found online at https://doi.org/10.1016/j.celrep.2019.10.112.

ACKNOWLEDGMENTS

This work was supported by the National Key Research and Development Program of China 2016YFC0905900 (G.Z. and S.Z.) and 2017YFC1001300 (G.Z.); the National Natural Science Foundation of China 81970878 (G.Z.), 31771130 (G.Z.), 81861128023 (G.Z.), and 31971178 (S.Z.); Natural Science Foundation of Shanghai grant 16ZR1448500 (S.Z.); the 2015 Thousand Youth Talents Plan of China (G.Z.); Shanghai Municipal Government; and ShanghaiTech University. The diffraction data were collected at BL41XU@ Spring-8. We thank Kazuya Hasegawa, Nobuhiro Mizuno, Takashi Kawamura, and Hironori Murakami for their help with data collection. We thank the Cloning Core, BV Core, and Purification Core of iHuman Institute for their help.

AUTHOR CONTRIBUTIONS

G.Z., project initiation and management; X.C., construct design, cloning, protein purification, data analysis, and manuscript writing; D.W., construct design, crystallization, and data collection; Y.X., functional studies; L.Q., data collection; Q.S., protein purification; L. Wu and G.W.H., data processing, structure determination, and refinement; Y.G. and S.Y., docking; Y.W., Q.Z., S.Z., R.C.S., and Z.J.L., structure analysis; L. Wang, functional assay; T.H. and H.T., synthesis of TC1515; Y. Sun, Y. Song, and L.H., radioligand binding assay; C.C. and J.Y., data analysis; L.Y. and Q.W., cloning; S.Z., D.W., and G.Z., project design, supervision, data analysis, and manuscript writing.

DECLARATION OF INTERESTS

The authors declare no competing interests.

Received: June 19, 2019
Revised: September 23, 2019
Accepted: October 28, 2019
Published: December 3, 2019

REFERENCES

Abraham, M.J., Murtola, T., Schulz, R., Pall, S., Smith, J.C., Hess, B., and Lindahl, E. (2015). GROMACS: High performance molecular simulations through multi-level parallelism from laptops to supercomputers. SoftwareX *1–2*, 19–25.

Adams, P.D., Afonine, P.V., Bunkóczi, G., Chen, V.B., Davis, I.W., Echols, N., Headd, J.J., Hung, L.W., Kapral, G.J., Grosse-Kunstleve, R.W., et al. (2010). PHENIX: a comprehensive Python-based system for macromolecular structure solution. Acta Crystallogr. D Biol. Crystallogr *66*, 213–221.

Ahlquist, R.P. (1948). A study of the adrenotropic receptors. Am. J. Physiol. *153*, 586–600.

Ahlquist, R.P. (1962). The adrenotropic receptor-detector. Arch. Int. Pharmacodyn. Ther. *139*, 38–41.

Ahlquist, R.P. (1967). Development of the concept of alpha and beta adrenotropic receptors. Ann. N Y Acad. Sci. *139*, 549–552.

Angelotti, T., Daunt, D., Shcherbakova, O.G., Kobilka, B., and Hurt, C.M. (2010). Regulation of G-protein coupled receptor traffic by an evolutionary conserved hydrophobic signal. Traffic *11*, 560–578.

Ban, T., Li, X., Ma, X., Yang, H., Song, Y., Sun, Y., Shen, M., Li, N., Zhang, M.Y., Ma, Y., et al. (2018). GPCR structure and function relationship: identification of a biased apelin receptor mutant. Biochem. J. *475*, 3813–3826.

Brede, M., Wiesmann, F., Jahns, R., Hadamek, K., Arnolt, C., Neubauer, S., Lohse, M.J., and Hein, L. (2002). Feedback inhibition of catecholamine release by two different alpha2-adrenoceptor subtypes prevents progression of heart failure. Circulation *106*, 2491–2496.

Brede, M., Nagy, G., Philipp, M., Sorensen, J.B., Lohse, M.J., and Hein, L. (2003). Differential control of adrenal and sympathetic catecholamine release by alpha 2-adrenoceptor subtypes. Mol. Endocrinol. *17*, 1640–1646.

Bücheler, M.M., Hadamek, K., and Hein, L. (2002). Two α(2)-adrenergic receptor subtypes, α(2A) and α(2C), inhibit transmitter release in the brain of gene-targeted mice. Neuroscience *109*, 819–826.

Cherezov, V., Rosenbaum, D.M., Hanson, M.A., Rasmussen, S.G., Thian, F.S., Kobilka, T.S., Choi, H.J., Kuhn, P., Weis, W.I., Kobilka, B.K., and Stevens, R.C. (2007). High-resolution crystal structure of an engineered human beta2-adrenergic G protein-coupled receptor. Science *318*, 1258–1265.

Cherezov, V., Hanson, M.A., Griffith, M.T., Hilgart, M.C., Sanishvili, R., Nagarajan, V., Stepanov, S., Fischetti, R.F., Kuhn, P., and Stevens, R.C. (2009). Rastering strategy for screening and centring of microcrystal samples of human membrane proteins with a sub-10 microm size X-ray synchrotron beam. J. R. Soc. Interface *6* (*Suppl 5*), S587–S597.

Chien, E.Y., Liu, W., Zhao, Q., Katritch, V., Han, G.W., Hanson, M.A., Shi, L., Newman, A.H., Javitch, J.A., Cherezov, V., and Stevens, R.C. (2010). Structure of the human dopamine D3 receptor in complex with a D2/D3 selective antagonist. Science *330*, 1091–1095.

Chotani, M.A., and Flavahan, N.A. (2011). Intracellular α(2C)-adrenoceptors: storage depot, stunted development or signaling domain? Biochim. Biophys. Acta *1813*, 1495–1503.

Chotani, M.A., Flavahan, S., Mitra, S., Daunt, D.A., and Flavahan, N.A. (1999). Silent alpha 2C-Adrenergic receptors enable cold-induced vasoconstriction in cutaneous arteries: A mechanism for Raynaud's phenomenon? Circulation *100*, 554.

Chotani, M.A., Flavahan, S., Mitra, S., Daunt, D., and Flavahan, N.A. (2000). Silent alpha(2C)-adrenergic receptors enable cold-induced vasoconstriction in cutaneous arteries. Am. J. Physiol. Heart Circ. Physiol. *278*, H1075–H1083.

Collaborative Computational Project, Number 4 (1994). The CCP4 suite: programs for protein crystallography. Acta Crystallogr. D Biol. Crystallogr *50*, 760–763.

Daunt, D.A., Hurt, C., Hein, L., Kallio, J., Feng, F., and Kobilka, B.K. (1997). Subtype-specific intracellular trafficking of alpha2-adrenergic receptors. Mol. Pharmacol. *51*, 711–720.

Emsley, P., Lohkamp, B., Scott, W.G., and Cowtan, K. (2010). Features and development of Coot. Acta Crystallogr. D Biol. Crystallogr. *66*, 486–501.

Filipeanu, C.M. (2015). Temperature-sensitive intracellular traffic of α2C-adrenergic receptor. Prog. Mol. Biol. Transl. Sci. *132*, 245–265.

Filipeanu, C.M., de Vries, R., Danser, A.H., and Kapusta, D.R. (2011). Modulation of α(2C) adrenergic receptor temperature-sensitive trafficking by HSP90. Biochim. Biophys. Acta *1813*, 346–357.

Filipeanu, C.M., Pullikuth, A.K., and Guidry, J.J. (2015). Molecular determinants of the human α2C-adrenergic receptor temperature-sensitive intracellular traffic. Mol. Pharmacol. *87*, 792–802.

Gilson, M.K., Sharp, K.A., and Honig, B.H. (1988). Calculating the electrostatic potential of molecules in solution: Method and error assessment. Journal of Computational Chemistry *9* (*4*), 327–335.

Haga, K., Kruse, A.C., Asada, H., Yurugi-Kobayashi, T., Shiroishi, M., Zhang, C., Weis, W.I., Okada, T., Kobilka, B.K., Haga, T., and Kobayashi, T. (2012). Structure of the human M2 muscarinic acetylcholine receptor bound to an antagonist. Nature *482*, 547–551.

Hein, L., Altman, J.D., and Kobilka, B.K. (1999). Two functionally distinct alpha2-adrenergic receptors regulate sympathetic neurotransmission. Nature *402*, 181–184.

Honda, M., Suzuki, M., Nakayama, K., and Ishikawa, T. (2007). Role of alpha2C-adrenoceptors in the reduction of skin blood flow induced by local cooling in mice. Br. J. Pharmacol. *152*, 91–100.

Hurt, C.M., Feng, F.Y., and Kobilka, B. (2000). Cell-type specific targeting of the alpha 2c-adrenoceptor. Evidence for the organization of receptor microdomains during neuronal differentiation of PC12 cells. J. Biol. Chem. *275*, 35424–35431.

Hwa, J., and Perez, D.M. (1996). The unique nature of the serine interactions for alpha 1-adrenergic receptor agonist binding and activation. J. Biol. Chem. *271*, 6322–6327.

Ishchenko, A., Wacker, D., Kapoor, M., Zhang, A., Han, G.W., Basu, S., Patel, N., Messerschmidt, M., Weierstall, U., Liu, W., et al. (2017). Structural insights into the extracellular recognition of the human serotonin 2B receptor by an antibody. Proc. Natl. Acad. Sci. USA *114*, 8223–8228.

Jeyaraj, S.C., Chotani, M.A., Mitra, S., Gregg, H.E., Flavahan, N.A., and Morrison, K.J. (2001). Cooling evokes redistribution of alpha2C-adrenoceptors from Golgi to plasma membrane in transfected human embryonic kidney 293 cells. Mol. Pharmacol. *60*, 1195–1200.

Kable, J.W., Murrin, L.C., and Bylund, D.B. (2000). In vivo gene modification elucidates subtype-specific functions of alpha(2)-adrenergic receptors. J. Pharmacol. Exp. Ther. *293*, 1–7.

Kabsch, W. (2010). Xds. Acta Crystallogr. D Biol. Crystallogr. *66*, 125–132.

Kruse, A.C., Hu, J., Pan, A.C., Arlow, D.H., Rosenbaum, D.M., Rosemond, E., Green, H.F., Liu, T., Chae, P.S., Dror, R.O., et al. (2012). Structure and dynamics of the M3 muscarinic acetylcholine receptor. Nature *482*, 552–556.

MacDonald, E., Kobilka, B.K., and Scheinin, M. (1997). Gene targeting—homing in on α2-adrenoceptor-subtype function. Trends Pharmacol. Sci. *18*, 211–219.

McCoy, A.J., Grosse-Kunstleve, R.W., Adams, P.D., Winn, M.D., Storoni, L.C., and Read, R.J. (2007). Phaser crystallographic software. J. Appl. Cryst. *40*, 658–674.

Michino, M., Beuming, T., Donthamsetti, P., Newman, A.H., Javitch, J.A., and Shi, L. (2015). What can crystal structures of aminergic receptors tell us about designing subtype-selective ligands? Pharmacol. Rev. *67*, 198–213.

Moura, E., Afonso, J., Hein, L., and Vieira-Coelho, M.A. (2006). Alpha2-adrenoceptor subtypes involved in the regulation of catecholamine release from the adrenal medulla of mice. Br. J. Pharmacol. *149*, 1049–1058.

Peng, Y., McCorvy, J.D., Harpsoe, K., Lansu, K., Yuan, S., Popov, P., Qu, L., Pu, M., Che, T., Nikolajsen, L.F., et al. (2018). 5-HT2C receptor structures reveal the structural basis of GPCR polypharmacology. Cell *172*, 719–730.e14.

Pettersen, E.F., Goddard, T.D., Huang, C.C., Couch, G.S., Greenblatt, D.M., Meng, E.C., and Ferrin, T.E. (2004). UCSF Chimera–a visualization system for exploratory research and analysis. J Comput Chem *25* (*13*), 1605–1612.

Rasmussen, S.G., DeVree, B.T., Zou, Y., Kruse, A.C., Chung, K.Y., Kobilka, T.S., Thian, F.S., Chae, P.S., Pardon, E., Calinski, D., et al. (2011). Crystal structure of the β2 adrenergic receptor-Gs protein complex. Nature *477*, 549–555.

Ring, A.M., Manglik, A., Kruse, A.C., Enos, M.D., Weis, W.I., Garcia, K.C., and Kobilka, B.K. (2013). Adrenaline-activated structure of β2-adrenoceptor stabilized by an engineered nanobody. Nature *502*, 575–579.

Sato, T., Kobayashi, H., Nagao, T., and Kurose, H. (1999). Ser203 as well as Ser204 and Ser207 in fifth transmembrane domain of the human beta2-adrenoceptor contributes to agonist binding and receptor activation. Br. J. Pharmacol. *128*, 272–274.

Sato, T., Baker, J., Warne, T., Brown, G.A., Leslie, A.G.W., Congreve, M., and Tate, C.G. (2015). Pharmacological analysis and structure determination of 7-methylcyanopindolol-bound β1-adrenergic receptor. Mol. Pharmacol. *88*, 1024–1034.

Shimamura, T., Shiroishi, M., Weyand, S., Tsujimoto, H., Winter, G., Katritch, V., Abagyan, R., Cherezov, V., Liu, W., Han, G.W., et al. (2011). Structure of the human histamine H1 receptor complex with doxepin. Nature *475*, 65–70.

Smart, O.S., Womack, T.O., Flensburg, C., Keller, P., Paciorek, W., Sharff, A., Vonrhein, C., and Bricogne, G. (2012). Exploiting structure similarity in refinement: automated NCS and target-structure restraints in BUSTER. Acta Crystallogr. D Biol. Crystallogr. *68*, 368–380.

Suryanarayana, S., and Kobilka, B.K. (1993). Amino acid substitutions at position 312 in the seventh hydrophobic segment of the beta 2-adrenergic receptor modify ligand-binding specificity. Mol. Pharmacol. *44*, 111–114.

Suryanarayana, S., Daunt, D.A., Von Zastrow, M., and Kobilka, B.K. (1991). A point mutation in the seventh hydrophobic domain of the alpha 2 adrenergic receptor increases its affinity for a family of beta receptor antagonists. J. Biol. Chem. *266*, 15488–15492.

Thal, D.M., Sun, B., Feng, D., Nawaratne, V., Leach, K., Felder, C.C., Bures, M.G., Evans, D.A., Weis, W.I., Bachhawat, P., et al. (2016). Crystal structures of the M1 and M4 muscarinic acetylcholine receptors. Nature *531*, 335–340.

Wang, S., Wacker, D., Levit, A., Che, T., Betz, R.M., McCorvy, J.D., Venkatakrishnan, A.J., Huang, X.P., Dror, R.O., Shoichet, B.K., and Roth, B.L. (2017). D_4 dopamine receptor high-resolution structures enable the discovery of selective agonists. Science *358*, 381–386.

Wang, S., Che, T., Levit, A., Shoichet, B.K., Wacker, D., and Roth, B.L. (2018). Structure of the D2 dopamine receptor bound to the atypical antipsychotic drug risperidone. Nature *555*, 269–273.

Warne, T., Edwards, P.C., Leslie, A.G., and Tate, C.G. (2012). Crystal structures of a stabilized β1-adrenoceptor bound to the biased agonists bucindolol and carvedilol. Structure *20*, 841–849.

Yin, W., Zhou, X.E., Yang, D., de Waal, P.W., Wang, M., Dai, A., Cai, X., Huang, C.Y., Liu, P., Wang, X., et al. (2018). Crystal structure of the human 5-HT_{1B} serotonin receptor bound to an inverse agonist. Cell Discov. *4*, 12.

Yuan, Y., Pei, J., and Lai, L. (2011). LigBuilder 2: a practical de novo drug design approach. J. Chem. Inf. Model. *51*, 1083–1091.

Yuan, Y., Pei, J., and Lai, L. (2013). Binding site detection and druggability prediction of protein targets for structure-based drug design. Curr. Pharm. Des. *19*, 2326–2333.

Zoete, V., Cuendet, M.A., Grosdidier, A., and Michielin, O. (2011). SwissParam: a fast force field generation tool for small organic molecules. J. Comput. Chem. *32*, 2359–2368.

STAR★METHODS

KEY RESOURCES TABLE

REAGENT or RESOURCE	SOURCE	IDENTIFIER
Chemicals, Peptides, and Recombinant Proteins		
EDTA-free complete protease inhibitor cocktail tablets	Roche	Cat#5056489001
Iodoacetamide	Sigma	Cat#I1149
N-Dodecyl-β-D-Maltoside, ANAGRADE	Anatrace	Cat#D310
Cholesterol hemisucinate (CHS)	Sigma	Cat#C6512
N-[4-(7-diethylamino-4-methyl-3-coumarinyl)phenyl]maleimide (CPM)	Invitrogen	Cat#D10251
TALON Superflow Metal Affinity Resin	Clontech	Cat#635670
1-Oleoyl-rac-glycerol (monoolein)	Sigma	Cat#M7765
Cholesterol	Sigma	Cat#C8667
RS79948 hydrochloride	Tocris	Cat#0987/50
JP1302 dihydrochloride	Abcam	Cat#ab141129
Norepinephrine (bitartrate monohydrate)	Medchemexpress	Cat#HY-13715B
L-epinephrine	Medchemexpress	Cat#HY-B0447B
UK14,304	Sigma	Cat#U104-5MG
Clonidine	Medchemexpress	Cat#HY-B0409A
Rauwolscine, [Methyl-3H]	Perkin Elmer	Cat.#NET722
OPC-28326	This paper	N/A
TC1515	This paper	N/A
Critical Commercial Assays		
D-Luciferin, Sodium Salt	BioVision	Cat#7902-10PK
Phusion High-Fidelity DNA Polymerase	NEB	Cat#M0530L
KOD -Plus-	TOYOBO	Cat#KOD-201
DpnI	NEB	Cat#R0176L
Deposited Data		
α_{2C}AR_RS79948 complex structure	This paper	PDB: 6KUW
Experimental Models: Cell Lines		
Spodoptera frugiperda (Sf9)	A gift from Dr. Beili Wu (SIMM, CAS)	N/A
Freestyle 293-F cells	Invitrogen	Cat#R790-07
CHO-K1	ATCC	Cat#CCL-61; RRID: CVCL_0214
Oligonucleotides		
Primers for site-direct mutagenesis on pcDNA 3.1-α_{2C}AR-WT. See Table S3		
Primers for site-direct mutagenesis on pcDNA 3.1-α_{2A}AR-WT. See Table S3		
Recombinant DNA		
pcDNA 3.1 (+) vector	Thermo Scientific	V79020
Software and Algorithms		
Chimera	Pettersen et al., 2004	http://www.cgl.ucsf.edu/chimera
DelPhi	Gilson et al., 1988	http://honig.c2b2.columbia.edu/delphi
Schrödinger Suite 2015-4	Schrödinger	https://www.schrodinger.com/
GROMACS 5.1.2	Abraham et al., 2015	http://www.gromacs.org
SwissParam	Zoete et al., 2011	http://www.swissparam.ch
XDS	Kabsch, 2010	http://xds.mpimf-heidelberg.mpg.de

(*Continued on next page*)

Continued

REAGENT or RESOURCE	SOURCE	IDENTIFIER
SCALA	Collaborative Computational Project, Number 4, 1994	http://www.ccp4.ac.uk/html/scala.html
Phaser	McCoy et al., 2007	http://www.phenix-online.org
Phenix	Adams et al., 2010	http://www.phenix-online.org
Buster	Smart et al., 2012	http://www.globalphasing.com/buster
COOT	Emsley et al., 2010	https://www2.mrc-lmb.cam.ac.uk/personal/pemsley/coot
Prism v.7.0	GraphPad Software Inc.	N/A
FlowJo® v.10.5.0	FlowJo, LLC	https://www.flowjo.com/solutions/flowjo
FluoView FV1000	Olympus - Life Science Solutions	https://www.olympus-lifescience.com/en/
Other		
CELLSTAR® microplate, 384 well, TC treated, white μClear®	Greiner	Cat#781098
DMEM/F-12 (1:1) cell culture media	Invitrogen	Cat#11330-057
Opti-MEM cell culture media	Invitrogen	Cat#11058-021
FreeStyle™ 293 Expression Medium	Life Technologies	Cat#12338-026
DMEM	Invitrogen	Cat#11965-118
MEM	Invitrogen	Cat#11095-098
Penicillin/Streptomycin	Invitrogen	Cat#15140-122
Bovine Serum Albumin, Fraction V, Cold-ethanol Precipitated	Fisher Scientific	Cat#BP1605100
Trypsin 0.5% EDTA	Invitrogen	Cat#25300-120
Cell Dissociation Buffer, Enzyme-Free, PBS based	GIBCO	Cat#13151014
Dulbecco's phosphate-buffered saline (DPBS)	Invitrogen	Cat#14190250
Hank's Balanced Salt Solution (HBSS)	Hyclone	Cat#SH30268.01
Fetal Bovine Serum (FBS)	Life Technologies	Cat#10099141
100kDa cutoff concentrators	Sartorius	Cat#VS0642
PD Minitrap G-25 coulmn	GE Healthcare	Cat#28-9180-07
96-well glass sandwich plates for LCP crystallization	NOVA	Cat#NOA90020

LEAD CONTACT AND MATERIALS AVAILABILITY

Further information and requests for resources and reagents should be directed to and will be fulfilled by the Lead Contact, Guisheng Zhong (zhongsh@shanghaitech.edu.cn). This study did not generate new unique reagents.

EXPERIMENTAL MODEL AND SUBJECT DETAILS

Cell Lines

Spodoptera frugiperda (Sf9) cells were used for α_{2C}AR expression and crystallization. Radioligand binding assay was performed with 293F cells expressing wild-type α_{2C}AR and engineered α_{2C}AR, respectively. CHO-K1 cells (ATCC) were used for Split luciferase biosensor cAMP assay.

Method Details

Synthesis of TC1515

Morpholine (2 equiv.) was added to a mixture of 4-fluoronitrobenzene (1 equiv.) and K_2CO_3 (1.5 equiv.) in dimethyl sulfoxide. The reaction mixture was stirred at 90°C and followed by TLC. After completion of the reaction, the mixture was diluted with ethyl acetate and washed with water, followed by brine. The ethyl acetate fraction was dried over Na_2SO_4 and concentrated. The crude products were purified by flash column chromatography to afford pure products. 4-(4-nitrophenyl)morpholine (1 equiv. in a mixture of methanol) was treated with 10% Pd-carbon (5% w/w). The reaction was subjected to hydrogenation under a hydrogen gas atmosphere at room temperature and the reaction was monitored by TLC. After completion of the reaction, the mixture was filtered through a Celite bed and concentrated in a vacuum to afford pure product in quantitative yields. A mixture of 4-morpholinoaniline, 9-chloroacridine and potassium carbonate in DMF solution was stirred at 50°C for 3 h. Ethyl acetate and water was added into the mixture to quench

the reaction, the aqueous layer was removed, and the organic layer was washed again with water. The ethyl acetate was evaporated, and the residue was purified by flash column chromatography to afford pure products.

Engineering of Human ADRA2C for Structure Determination

The human WT ADRA2C (UniProtKB-P18825) gene was synthesized using GenScript with flanking restriction sites AscI at the 5′ end and FseI at the 3′ end. The expression vector was a modified pFastBac1 vector (*Invitrogen*) containing an expression cassette with an HA signal sequence followed by a FLAG tag at the N terminus and a PreScission protease site followed by a 10xHis tag at the C terminus. A DNA fragment corresponding to residues 29-458 of ADRA2C_HUMAN was cloned into the site between AscI and FseI. ICL3 region (242-371) was replaced by a PGS fusion protein that was generated by the 196-amino-acid coding sequence of *P. abysii* glycogen synthase (PDB accession 2BFW). Three mutations I139A, V122W, F391W were introduced into this construct by standard QuickChange PCR protocol.

Protein Expression in sf9 Insect Cell Line

The Bac-to-Bac Baculovirus Expression System (*Invitrogen*) was used to generate high-titer recombinant baculovirus (> 10^9 viral particles per ml). Recombinant baculovirus was produced by transfecting recombinant bacmids (2.5-5 mg) into *Spodoptera frugiperda* (Sf9) cells (2.5 mL, density of 10^6 cells per mL) using 5 mL of X-tremeGENE HP DNA Transfection Reagent (Roche) and Transfection Medium (Expression Systems). After 4 days of shaking at 27°C, P0 viral stock ($\sim 10^9$ virus particles per mL) was harvested as the supernatant of the cell suspension to produce high-titer viral stock. Viral titers were analyzed by flow cytometry on cells stained with gp64-PE antibody (Expression Systems). α_{2C}AR was expressed by infecting Sf9 cells at a cell density of 2-3x10^6 cells per ml with P1 virus at MOI (multiplicity of infection) of 5. Cells were harvested by centrifugation 48 h post infection and stored at −80°C for future use.

Protein Purification

Thawed insect cell membranes were disrupted in a hypotonic buffer containing 10 mM $MgCl_2$, 20 mM KCl, 10 mM HEPES (pH 7.5), and EDTA-free complete protease inhibitor cocktail tablets (Roche). The isolated raw membranes were extensively washed by twice repeated centrifugation in the same hypotonic buffer. Subsequently, soluble and membrane-associated proteins were removed in a high osmotic buffer containing 10 mM $MgCl_2$, 20 mM KCl, 1.0 M NaCl, 10 mM HEPES (pH 7.5), and EDTA-free complete protease inhibitor cocktail tablets (three times). Purified membranes were flash-frozen in liquid nitrogen and stored at −80°C for further use.

Purified membranes were thawed at room temperature and incubated in the presence of 50 μM RS79948 and protease inhibitor cocktail at 4°C for 2 h. The membranes were incubated with 2.0 mg/mL iodoacetamide (Sigma) for 30 min and were solubilized in the buffer containing 50 mM HEPES (pH 7.5), 2% (w/v) n-dodecyl-beta-D-maltopyranoside (DDM, Anatrace), 0.2% (w/v) cholesterol hemisuccinate (CHS, Sigma-Aldrich), and 150 mM NaCl, at 4°C for 2.5 h. The solubilized proteins in the supernatants were isolated by high-speed centrifugation (Beckman), and then incubated at 4°C overnight with TALON IMAC resin (Clontech), 500 mM NaCl, and 20 mM imidazole as the final buffer concentration. The resin was washed with 10 column volumes of washing buffer I containing 50 mM HEPES (pH 7.5), 0.1% (w/v) DDM, 0.02% (w/v) CHS, 500 mM NaCl, 10% (v/v) glycerol, 20 mM imidazole, and 50 μM RS79948, and 6 column volumes of washing buffer II containing 50mM HEPES (pH 7.5), 0.02% (w/v) DDM, 0.004% (w/v) CHS, 500 mM NaCl, 10% (v/v) glycerol, and 50 μM RS79948 without imidazole. The protein was eluted using 4 column volumes of elution buffer containing 50 mM HEPES (pH 7.5), 0.02% (w/v) DDM, 0.004% (w/v) CHS, 500 mM NaCl, 10% (v/v) glycerol, 250 Mm imidazole, and 50 μM RS79948. The protein sample was concentrated to 30 mg/mL using a 100 kDa cut-off concentrator (Sartorius) for crystallization trials. The protein yield and monodispersity were measured by aSEC.

Lipidic Cubic Phase Crystallization

The purified α_{2C}AR protein in complex with RS79948 was screened for crystallization in lipidic cubic phase (LCP) with mixed molten lipid (90% (w/v) monoolein and 10% (w/v) cholesterol) at a protein/lipid ratio of 2:3 (v/v) using a mechanical syringe mixer. LCP crystallization trials were set up using an NT8-LCP crystallization robot (Formulatrix). 96-well glass sandwich plates were incubated at 20°C in an automatic incubator/imager (RockImager 1000, Formulatrix) and imaged. Crystals were obtained in sodium phosphate monobasic (0.1M), HEPES pH6.5-6.9 (0.1M), PEG400 24%–35%, and grew to full size in around 3 day. The crystals were harvested using micromounts (MiTeGen) and flash-frozen in liquid nitrogen.

Data Collection and Structure Determination

X-ray diffraction data of α_{2C}AR RS79948 crystals were collected at beam line BL41XU at SPring-8, Japan, using Eiger 6M detector (X-ray wavelength 1.0000 A°). The data collection strategy was designed based on rastering results as previously described (Cherezov et al., 2009). Diffraction images were indexed, integrated, and scaled using XDS (Kabsch, 2010). Initial phases were obtained by the molecular replacement-(MR) method with Phaser (McCoy et al., 2007). Refinement was carried out with Buster (Smart et al., 2012) iteratively followed by manual examination and adjustments of the refined coordinates in the program COOT (Emsley et al., 2010) using both |Fo|-|Fc| and 2|Fo|-|Fc| electron density maps and omit maps.

Radioligand Binding Assay

Cell membranes from 293F cells expressing wild-type or the engineered α_{2C}AR receptors were prepared (Ban et al., 2018). After protein concentration determined using BCA method, aliquoted membrane preparations were stored at −80°C. In saturation binding assay, 20 μg WT type or 10 μg mutant membrane was incubated with serial of concentrations of [Methyl-^{3}H]-Rauwolscine (Perkin Elmer, Cat.#NET722) in the binding buffer (50 mM HEPES pH 7.4, 5 mM $MgCl_2$, 1 mM $CaCl^2$, 0.2% BSA) in a total volume of 120 μl. In the competition binding assay, the membrane was incubated with 15 nM [^{3}H]-Rauwolscine in the presence of serial concentration of compounds. The binding reaction mixture was incubated at room temperature in a 96-well plate for 2 h while gently shaking, then was transferred to PEI pre-coated UniFilter GF/B filtration plate and filtered using FilterMate Universal Harvester (Perkin Elmer). The filtration plate was washed quickly three times with ice-cold washing buffer (50 mM HEPES pH 7.4, 500 mM NaCl, 0.1% BSA) then dried at 37°C for 2 h. Scintillation cocktail was added to each well, and radioactivity was counted in MicroBeta Trilux (Perkin Elmer).

Cell Culture and Transfection

To determine GPCR-mediated cAMP production, Promega's split luciferase-based GloSensor cAMP biosensor technology was used. CHO-K1 cells (ATCC) were maintained in F-12 supplemented with 10% FBS and 1% penicillin/streptavidin. When cells reached 70% confluence in a10 cm dish, 1 μg of DNA and 1 μg of GloSensor cAMP DNA were co-transfected by TransIT 2020 (Mirus bio). On the following day, cells were seeded into 384-well white clear-bottom cell culture plates (Greiner) at a density of 10-15,000 cells in 40 μL growth medium per well. The plates were used in assays the next day.

Split Luciferase Biosensor cAMP Assay

After supernatant was removed from 384 well plates, the wells were loaded for 60 min at 37°C with 20 μL of 2 mg/ml Luciferin prepared in HBSS with 0.1% BSA (pH 7.4). All the following steps were carried out at room temperature. To measure agonist activity at α_{2C}AR, 10 μL 4x test drug solution was added with 15 min incubation before the addition of 10 μL of forskolin (Sigma Aldrich) at a final concentration of 20 μM, followed by the counting of the plate for chemiluminescence after 15 min. To measure antagonist activity, cells were preincubated with test drug for 15 min before a 4x 350nM of UK 14,304 and forskolin at a final concentration of 20 μM were added. Counting was undertaken after 15 min. Chemiluminescence signal was measured on EnVision plate reader (Perkin Elmer).

Epinephrine, JP1302, and OPC-28326 Docking to α_{2A}AR and α_{2C}AR

We prepared structures of α_{2A}AR-RS79948 and α_{2C}AR-RS79948 using Protein Preparation Wizard in Maestro (Schrödinger LLC, New York, NY, USA). Proteins were pre-processed with default options in "Import and Process" panel. For epinephrine, JP1302 and OPC-28326, ionization and conformation states were determined using OPLS3 force field by LigPrep Script in Maestro. The docking of epinephrine, JP1302 and OPC-28326 was performed using the Induced Fit Docking (IFD) program (Schrödinger LLC, New York, NY, USA) with default parameters and a grid box defined by the molecule RS79948's position in the crystal structure. Finally, we selected the model based on our knowledge (i.e., there must be a salt bridge between ligand and D3.32 in protein) from the IFD results with good scores.

Calculation of Binding Pocket's Volume

The calculation was performed using the program Cavity (Yuan et al., 2011, 2013) in "large" mode. The program uses a pretrained model to find atoms that could form a closed pocket. After calculation, Cavity returns a series of pocket pdb files and the vacant files. In the pdb files, the pocket is represented using the least number of closest atoms. In the vacant file, the space inside the pocket is filled with cubic boxes. By counting the number of cubic boxes, the program returns a volume value. The pocket with ligand inside was selected and pocket volume was read from the corresponding vacant file.

Calculation of RMSD

The RMSD values of Cα atoms in transmembrane helices were calculated using UCSF chimera for edge attribute. In total 192 residues were included: BWN 1.35-57, 2.37-63, 3.22-56, 4.39-63, 5.36-65, 6.33-59, 7.31-55.

QUANTIFICATION AND STATISTICAL ANALYSIS

The data obtained for individual experimental pEC_{50} between WT and mutant α_{2C}ARs are presented as mean ± SEM ($N \geq 3$) in Prism 7 (GraphPad, La Jolla, CA). Statistical analyses comparing pEC_{50} between α_{2C}AR WT and mutants were conducted using two-way ANOVA in Prism 7. K_d values for saturation binding assay and K_i values for radioligand competition binding assay are presented as mean ± SD (N = 3).

DATA AND CODE AVAILABILITY

The accession number for the coordinates and structure factors of α_{2C}AR_RS79948 is PDB: 6KUW.